JOURNAL OF GUIDANCE, CONTROL, AND DYNAMICS
Vol. 27, No. 5, September–October 2004

Linear Theory of a Rotating Internal Part Projectile Configuration in Atmospheric Flight

Geoffrey Frost* and Mark Costello†
Oregon State University, Corvallis, Oregon 97331

Dynamic modeling of the atmospheric flight mechanics of a projectile equipped with an internal rotating disk is investigated, and a modified projectile linear theory is established for this configuration. To model this type of projectile requires alteration of several of the coefficients of the epicyclic dynamics leading to changes in the fast and slow epicyclic modes. A study of the frequency and damping properties of the epicyclic modes is conducted by the systematic variation of disk orientation, location, mass, and rotational speed. It is shown that the presence of an internal rotating disk can causes substantial changes in the epicyclic dynamics, including instability, in some configurations.

Nomenclature

$\boldsymbol{a}_{C/I}$	=	translational acceleration vector of two-body system with respect to the inertial frame
$\boldsymbol{a}_{D/I}$	=	translational acceleration vector of disk mass center with respect to the inertial frame
$\boldsymbol{a}_{P/I}$	=	translational acceleration vector of projectile body mass center with respect to the inertial frame
C_{DD}	=	roll moment aerodynamic coefficient for the projectile body
C_{LP}	=	roll damping moment aerodynamic coefficient for the projectile body
C_{MQ}	=	pitch damping moment aerodynamic coefficient for the projectile body
C_{NA}	=	normal force aerodynamic coefficient for the projectile body
C_{X0}	=	zero yaw axial force aerodynamic coefficient for the projectile body
C_{X2}	=	yaw drag axial force aerodynamic coefficient for the projectile body
C_{YPA}	=	Magnus force aerodynamic coefficient for the projectile body
$\boldsymbol{F}_A$	=	aerodynamic forces vector
$\boldsymbol{F}_R$	=	reaction force vector
H_{Dx}, H_{Dy}, H_{Dz}	=	angular momentum derivative vector components of the projectile body expressed in the body frame
$\boldsymbol{H}_{D/I}$	=	angular momentum vector of the disk body about disk mass center with respect to the inertial frame
H_{Px}, H_{Py}, H_{Pz}	=	angular momentum derivative vector components of the projectile body expressed in the body frame
$\boldsymbol{H}_{P/I}$	=	angular momentum vector of the projectile body about projectile mass center with respect to the inertial frame
$\tilde{H}_{Dx}, \tilde{H}_{Dy}, \tilde{H}_{Dz}$	=	angular momentum derivative vector components of the projectile body expressed in the no-roll frame
$\tilde{H}_{Px}, \tilde{H}_{Py}, \tilde{H}_{Pz}$	=	angular momentum derivative vector components of the projectile body expressed in the no-roll frame
$\boldsymbol{I}_B, \boldsymbol{J}_B, \boldsymbol{K}_B$	=	body frame unit vectors
I_D	=	mass moment of inertia of the disk body about its mass center with respect to the disk frame
I_E	=	nominal mass moment of inertia of the projectile body about its mass center with respect to the body frame
$\boldsymbol{I}_I, \boldsymbol{J}_I, \boldsymbol{K}_I$	=	inertial frame unit vectors
$\boldsymbol{I}_N, \boldsymbol{J}_N, \boldsymbol{K}_N$	=	no-roll frame unit vectors
I_P	=	mass moment of inertia of the projectile body about its mass center with respect to the body frame
L_A, M_A, N_A	=	total aerodynamic moment vector components expressed in the body frame
L_R, M_R, N_R	=	reaction moment components due to cross product of distance vector from projectile center of mass to disk center of mass with reaction force vector expressed in the body frame
$\tilde{L}, \tilde{M}, \tilde{N}$	=	total aerodynamic moment vector components expressed in the no-roll frame
$\tilde{L}_A, \tilde{M}_A, \tilde{N}_A$	=	total aerodynamic moment vector components expressed in the no-roll frame
$\tilde{L}_R, \tilde{M}_R, \tilde{N}_R$	=	reaction moment components due to cross product of distance vector from projectile center of mass to disk center of mass with reaction force vector expressed in the no-roll frame
$\boldsymbol{M}_A$	=	total aerodynamic moment vector
$\boldsymbol{M}_R$	=	reaction moment vector
m_C	=	two-body system mass
m_D	=	disk body mass
m_E	=	nominal projectile mass
m_P	=	projectile body mass
p, q, r	=	roll, pitch, and yaw components of the angular velocity vector of projectile body expressed in the body frame
$\tilde{p}, \tilde{q}, \tilde{r}$	=	roll, pitch, and yaw components of the angular velocity vector of projectile body expressed in the no-roll frame
$\boldsymbol{r}_{C\to D}$	=	distance vector from composite body center of mass to disk center of mass
$\boldsymbol{r}_{C\to P}$	=	distance vector from composite body center of mass to projectile center of mass
$\boldsymbol{r}_{P\to D}$	=	distance vector from projectile center of mass to disk center of mass

Received 10 March 2003; revision received 13 October 2003; accepted for publication 11 November 2003.

*Graduate Research Assistant, Department of Mechanical Engineering. Member AIAA.

†Associate Professor, Department of Mechanical Engineering. Member AIAA.

T_D = transformation matrix from the disk frame to the body frame
T_N = transformation matrix from the body frame to the no-roll frame
T_P = transformation matrix from the body frame to the inertial frame
u, v, w = translational velocity components of the two-body system center of mass resolved in the body frame
$\tilde{u}, \tilde{v}, \tilde{w}$ = translational velocity components of the two-body system center of mass resolved in the no-roll frame
V = velocity magnitude
$\boldsymbol{v}_{C/I}$ = translational velocity vector of two-body system with respect to the inertial frame
$\boldsymbol{W}_C$ = weight vector of two-body system
$\boldsymbol{W}_D$ = weight vector of disk body
$\boldsymbol{W}_P$ = weight vector of projectile body
X_A, Y_A, Z_A = aerodynamic force vector components expressed in the body frame
X_W, Y_W, Z_W = projectile weight vector components expressed in the body frame
$\tilde{X}, \tilde{Y}, \tilde{Z}$ = total external force components on the projectile body expressed in the no-roll frame
$\tilde{X}_A, \tilde{Y}_A, \tilde{Z}_A$ = aerodynamic force vector components expressed in the no-roll frame
$\tilde{X}_W, \tilde{Y}_W, \tilde{Z}_W$ = projectile weight vector components expressed in the no-roll frame
x, y, z = position vector components of the two-body system center of mass expressed in the inertial frame
x_D, y_D, z_D = body frame components of distance vector from projectile center of base to disk center of mass
x_E, y_E, z_E = nominal body frame components of distance vector from projectile center of base to projectile center of mass
x_P, y_P, z_P = body frame components of distance vector from projectile center of base to projectile center of mass
x_{PA}, y_{PA}, z_{PA} = no-roll frame components of distance vector from projectile center of mass to center of pressure
x_{PD}, y_{PD}, z_{PD} = body frame components of distance vector from projectile center of mass to disk center of mass
x_{PM}, y_{PM}, z_{PM} = no-roll frame components of distance vector from projectile center of mass to Magnus center of pressure
α = longitudinal aerodynamic angle of attack
$\boldsymbol{\alpha}_{P/I}$ = angular acceleration vector of projectile body with respect to the inertial frame
β = lateral aerodynamic angle of attack
ρ = density of air
ϕ, θ, ψ = Euler roll, pitch, and yaw angles
ϕ_D, θ_D = disk reference frame orientation angles
$\boldsymbol{\omega}_{B/I}$ = angular velocity vector of projectile body with respect to the inertial frame
$\boldsymbol{\omega}_{D/I}$ = angular velocity vector of disk body with respect to the inertial frame
$\boldsymbol{\omega}_{D/P}$ = angular velocity vector of disk body with respect to the projectile body frame
$\boldsymbol{\omega}_{N/I}$ = angular velocity vector of no-roll reference frame with respect to the inertial frame

Introduction

MANY conventional projectile configurations contain internal parts that move slightly in-flight in some way, shape, or form. Fuze mechanisms used on some indirect fire ammunition employ a rotor that is permitted to move slightly with respect to the main projectile body. Submunitions deployed from indirect fire projectiles are keyed into place inside the round; however, small relative motion between parts occurs. These configurations can experience dynamic instability typified by large loss in range and large spin decay.[1] Soper evaluated the stability of a spinning projectile that contains a cylindrical mass fitted loosely into a cylindrical cavity.[2] The cylinder is constrained to spin with the main body projectile. It is shown that an unstable coning motion exists in which spin decay and cone angle grow proportionally to the friction coefficient between the mass and cavity and the maximum cant angle between the mass and the projectile. With use of a similar geometric configuration, Murphy developed a quasi-linear solution for a projectile with an internal moving part.[3] The solution provided an explanation of the unusual flight behavior exhibited by four projectiles that all contained parts with slight relative motion between components. Later, D'Amico performed a detailed series of experiments where a projectile with a loose internal part was driven by the rotor of a freely gimbaled gyroscope.[4] The gyroscope yaw history and the orbital motion of the loose part were measured and used to predict the moment and resulting yaw growth caused by the loose part. Hodapp[5] expanded the work of Soper[2] and Murphy[3] by considering a projectile configuration with a partially restrained internal member with a mass center offset. Results of this study[5] indicate that small mass center offset of the partially restrained internal member can reduce the instability caused by the loose internal part.

New projectiles configurations have emerged that contain multiple moving parts that are fundamental to the basic design and operation of the projectile. The gimbal nose projectile configuration is an example of one such configuration. It consists of a standard projectile shape with a nose section that is free to rotate with respect to the main body. Goddard[6] originally conceived of this device for aircraft control, and later Barrett and Stutts[7] considered this mechanism for active control of munitions. Schmidt and Donovan[8] as well as Costello and Agarwalla[9] showed that dispersion of a fin-stabilized direct fire projectile could be reduced by more than 50% using a passive gimbal nose to reduce significantly aerodynamic jump. Another multiple component configuration is the dual-spin projectile, which consists of forward and aft sections connected through a bearing, which allows different spin rates for each section. Smith et al.[10] used a dual-spin projectile for active control of an artillery shell by mounting canards on the forward section of the projectile. The forward section was roll stabilized to aid the functionality of the canards, whereas the aft section provided spin stability. Costello and Peterson[11] developed a linear theory for dual-spin projectiles that predicts stability for this configuration, whereas Burchett et al.[12] predicted swerve of a dual-spin projectile caused by lateral pulse jets.

An internal rotating disk is an important dynamic component of some new projectile configurations. For example, a new concept for generating real-time bomb damage information relies on releasing a relatively small sensor projectile that is tethered to a parent bomb. As the two projectiles separate, a reel on the parent munition spins. In another application, active trajectory control is achieved by controlling the spin rate of the external projectile body, thus, predictably changing the aerodynamic loads. To implement this control concept requires an internal rotating disk. In these cases, weapon system designers require guidance on the effect of the rotating internal part as well as guidance on how to configure such a system optimally. The work reported here sheds light on these matters by first developing a projectile linear theory specific to projectiles with an internal rotating disk. Unlike previous work, the model is valid for large disk to projectile mass ratio, arbitrary orientation of the disk, and arbitrary placement of the disk within the projectile. The effect of physical parameters such as orientation, placement, mass, and speed of the rotating disk on the epicyclic modes of vibration is examined.

Rotating Internal Part Projectile Dynamic Model

A projectile containing an axisymmetric rotating internal part that spins at a constant rate Ω is considered, as shown in Fig. 1. The mathematical model describing the motion of the projectile allows for three translational and three rotational rigid-body degrees of freedom. To develop the dynamic equations of motion for these

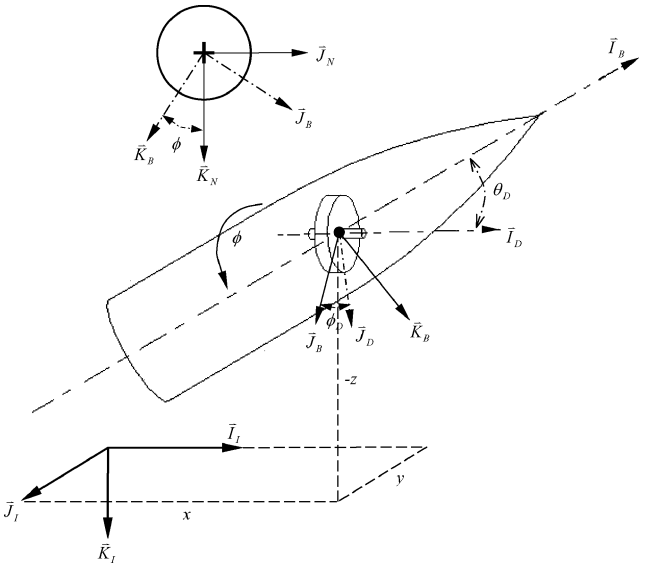

Fig. 1 Position coordinates schematic of a rotating internal part projectile.

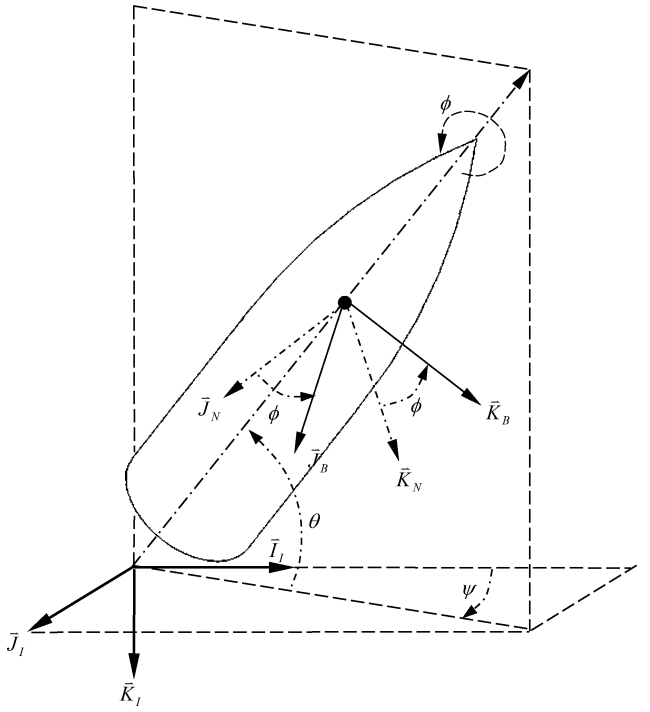

Fig. 2 Attitude coordinates schematic of a rotating internal part projectile.

six degrees of freedom, three separate reference frames are used as shown in Fig. 1. The ground surface is used as an inertial reference frame with $\boldsymbol{K}_I$ positive down. A body frame is fixed on the projectile at the mass center of the two-body system with $\boldsymbol{I}_B$ positive out the nose of the projectile. Because of the axisymmetric nature of the rotating internal part, the mass center of the internal part is fixed with respect to the body frame. The disk is considered to have a known constant spin rate, and its axis of spin is specified in the body frame by a set of direction cosine elements.

The three translational degrees of freedom are the three components of the two-body, mass center position vector:

$$\boldsymbol{r}_{O\to C} = x\boldsymbol{I}_I + y\boldsymbol{J}_I + z\boldsymbol{K}_I \tag{1}$$

A sequence of rotations from the inertial frame to the projectile frame is defined by a set of body-fixed rotations that are ordered in the conventional manner as shown in Fig. 2. The three rotational

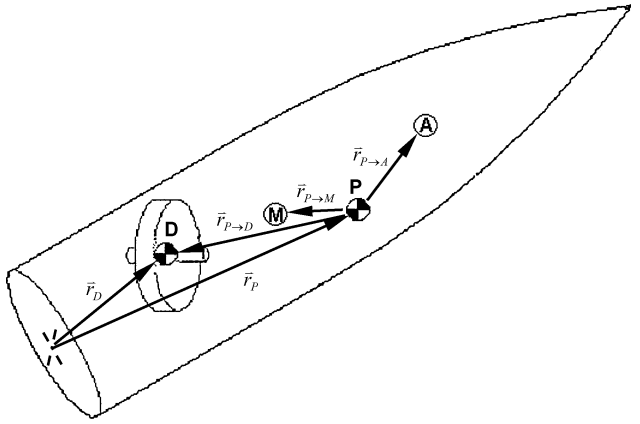

Fig. 3 Rotating internal part projectile geometry.

degrees of freedom are the Euler roll angle ϕ, pitch angle θ, and yaw angle ψ. In the normal process of simplifying the equations of motion using projectile linear theory, an intermediate frame is utilized, namely, the no-roll frame, defined as an intermediate frame before roll angle rotation. Figure 3 shows the relative locations of the projectile and disk centers of gravity and the projectile body centers of pressure.

The kinematic differential equations define 6 of the 12 dynamic equations needed to describe the motion of the states: x, y, z, φ, θ, and ψ. The no-roll variables, $\tilde{u}$, $\tilde{v}$, $\tilde{w}$, $\tilde{p}$, $\tilde{q}$, and $\tilde{r}$, are chosen for the remaining 12 state variables. The transformation from the no-roll frame N to the inertial frame I is

$$\begin{Bmatrix}\boldsymbol{I}_I\\ \boldsymbol{J}_I\\ \boldsymbol{K}_I\end{Bmatrix} = \begin{bmatrix} c_\theta c_\psi & -s_\psi & s_\theta c_\psi \\ c_\theta s_\psi & c_\psi & s_\theta s_\psi \\ -s_\theta & 0 & c_\theta \end{bmatrix} \begin{Bmatrix}\boldsymbol{I}_N\\ \boldsymbol{J}_N\\ \boldsymbol{K}_N\end{Bmatrix} = [T_N] \begin{Bmatrix}\boldsymbol{I}_N\\ \boldsymbol{J}_N\\ \boldsymbol{K}_N\end{Bmatrix} \tag{2}$$

whereas the transformation from the projectile body frame B to the no-roll frame N is

$$\begin{Bmatrix}\boldsymbol{I}_N\\ \boldsymbol{J}_N\\ \boldsymbol{K}_N\end{Bmatrix} = \begin{bmatrix} 1 & 0 & 0 \\ 0 & c_\phi & -s_\phi \\ 0 & s_\phi & c_\phi \end{bmatrix} \begin{Bmatrix}\boldsymbol{I}_B\\ \boldsymbol{J}_B\\ \boldsymbol{K}_B\end{Bmatrix} = \left[T_\phi^T\right] \begin{Bmatrix}\boldsymbol{I}_B\\ \boldsymbol{J}_B\\ \boldsymbol{K}_B\end{Bmatrix} \tag{3}$$

leading to the transformation from the body frame B to the inertial frame I described by

$$\begin{Bmatrix}\boldsymbol{I}_I\\ \boldsymbol{J}_I\\ \boldsymbol{K}_I\end{Bmatrix} = \begin{bmatrix} c_\theta c_\psi & s_\phi s_\theta c_\psi - c_\phi s_\psi & c_\phi s_\theta c_\psi + s_\phi s_\psi \\ c_\theta s_\psi & s_\phi s_\theta s_\psi + c_\phi c_\psi & c_\phi s_\theta s_\psi - s_\phi c_\psi \\ -s_\theta & s_\phi c_\theta & c_\phi c_\theta \end{bmatrix} \begin{Bmatrix}\boldsymbol{I}_B\\ \boldsymbol{J}_B\\ \boldsymbol{K}_B\end{Bmatrix}$$

$$= [T_B] \begin{Bmatrix}\boldsymbol{I}_B\\ \boldsymbol{J}_B\\ \boldsymbol{K}_B\end{Bmatrix} \tag{4}$$

In the preceding equations and the equations to be shown later, the standard shorthand notation for trigonometric functions is used: $\sin(\alpha) \equiv s_\alpha$, $\cos(\alpha) \equiv c_\alpha$, and $\tan(\alpha) \equiv t_\alpha$.

The mass center velocity vector of the two-body system is defined in each of the reference frames already discussed,

$$\boldsymbol{v}_{C/I} = \tilde{u}\boldsymbol{I}_N + \tilde{v}\boldsymbol{J}_N + \tilde{w}\boldsymbol{K}_N = u\boldsymbol{I}_B + v\boldsymbol{J}_B + w\boldsymbol{K}_B = \dot{x}\boldsymbol{I}_I + \dot{y}\boldsymbol{J}_I + \dot{z}\boldsymbol{K}_I \tag{5}$$

as is the angular velocity vector of the projectile body,

$$\boldsymbol{\omega}_{B/I} = \tilde{p}\boldsymbol{I}_N + \tilde{q}\boldsymbol{J}_N + \tilde{r}\boldsymbol{K}_N = p\boldsymbol{I}_B + q\boldsymbol{J}_B + r\boldsymbol{K}_B \tag{6}$$

and the angular velocity vector of the no-roll reference frame,

$$\boldsymbol{\omega}_{N/I} = -\tilde{r}t_\theta\boldsymbol{I}_N + \tilde{q}\boldsymbol{J}_N + \tilde{r}\boldsymbol{K}_N \tag{7}$$

The angular velocity vector of the internal rotating part with respect to the inertial frame is found by summing the angular velocity vector of the projectile body with respect to the inertial frame with the angular velocity vector of the internal rotating part with respect to the projectile body frame,

$$\boldsymbol{\omega}_{D/I} = \boldsymbol{\omega}_{B/I} + \boldsymbol{\omega}_{D/B} \tag{8}$$

where the angular velocity vector of the internal rotating part with respect to the projectile body frame is

$$\boldsymbol{\omega}_{D/P} = n_x \Omega \boldsymbol{I}_B + n_y \Omega \boldsymbol{J}_B + n_z \Omega \boldsymbol{K}_B \tag{9}$$

where

$$\begin{Bmatrix} n_x \\ n_y \\ n_z \end{Bmatrix} = \begin{Bmatrix} c_{\theta_D} \\ s_{\phi_D} s_{\theta_D} \\ -c_{\phi_D} s_{\theta_D} \end{Bmatrix} \tag{10}$$

Applying the transformation given in Eq. (2) to the mass center velocity components expressed in the no-roll reference frame yields

$$\begin{Bmatrix} \dot{x} \\ \dot{y} \\ \dot{z} \end{Bmatrix} = \begin{bmatrix} c_\theta c_\psi & -s_\psi & s_\theta c_\psi \\ c_\theta s_\psi & c_\psi & s_\theta s_\psi \\ -s_\theta & 0 & c_\theta \end{bmatrix} \begin{Bmatrix} \tilde{u} \\ \tilde{v} \\ \tilde{w} \end{Bmatrix} \tag{11}$$

Equating the projectile angular velocity vectors described using no-roll frame components and using Euler angle rates generates

$$\begin{Bmatrix} \dot{\phi} \\ \dot{\theta} \\ \dot{\psi} \end{Bmatrix} = \begin{bmatrix} 1 & 0 & t_\theta \\ 0 & 1 & 0 \\ 0 & 0 & 1/c_\theta \end{bmatrix} \begin{Bmatrix} \tilde{p} \\ \tilde{q} \\ \tilde{r} \end{Bmatrix} \tag{12}$$

The kinetic differential equations are derived by separating the two-body system at the disk axle connection point and considering the reaction forces and moments associated with each individual part. A constraint force $\boldsymbol{F}_R$ and a constraint moment $\boldsymbol{M}_R$, applied at the disk center of gravity, couple the disk and projectile bodies. Equations (13) and (14) give the translational kinetic differential equations for each body,

$$m_D \boldsymbol{a}_{D/I} = \boldsymbol{F}_R + \boldsymbol{W}_D \tag{13}$$

$$m_P \boldsymbol{a}_{P/I} = -\boldsymbol{F}_R + \boldsymbol{W}_P + \boldsymbol{F}_A \tag{14}$$

Summing Eqs. (13) and (14) yields the expression for the translational dynamic equation of motion for the two-body system,

$$m_C \boldsymbol{a}_{C/I} = \boldsymbol{F}_A + \boldsymbol{W}_C \tag{15}$$

where

$$m_C \boldsymbol{a}_{C/I} = m_D \boldsymbol{a}_{D/I} + m_P \boldsymbol{a}_{P/I} \tag{16}$$

$$\boldsymbol{W}_C = \boldsymbol{W}_P + \boldsymbol{W}_D \tag{17}$$

$$\boldsymbol{a}_{C/I} = \frac{{}^N \mathrm{d}\boldsymbol{V}_{C/I}}{\mathrm{d}t} + \boldsymbol{\omega}_{N/I} \times \boldsymbol{V}_{C/I} \tag{18}$$

The constraint force is obtained by subtracting Eq. (14) from Eq. (13),

$$\boldsymbol{F}_R = (\boldsymbol{a}_{D/I} - \boldsymbol{a}_{P/I} + \boldsymbol{F}_A/m_P)[m_D m_P/(m_D + m_P)] \tag{19}$$

The acceleration of the mass center of the disk, $\boldsymbol{a}_{D/I}$, and the acceleration of the mass center of the projectile, $\boldsymbol{a}_{P/I}$, can be expressed in terms of the acceleration of the composite body mass center by using the formula for two points fixed on a rigid body.

$$\boldsymbol{a}_{D/I} = \boldsymbol{a}_{C/I} + \boldsymbol{\alpha}_{B/I} \times \boldsymbol{r}_{C\to D} + \boldsymbol{\omega}_{B/I} \times (\boldsymbol{\omega}_{B/I} \times \boldsymbol{r}_{C\to D}) \tag{20}$$

$$\boldsymbol{a}_{P/I} = \boldsymbol{a}_{C/I} + \boldsymbol{\alpha}_{B/I} \times \boldsymbol{r}_{C\to P} + \boldsymbol{\omega}_{B/I} \times (\boldsymbol{\omega}_{B/I} \times \boldsymbol{r}_{C\to P}) \tag{21}$$

After these expressions are substituted into Eq. (19), the constraint force is expressed in the following manner:

$$\boldsymbol{F}_R = [\boldsymbol{\alpha}_{B/I} \times \boldsymbol{r}_{P\to D} + \boldsymbol{\omega}_{B/I} \times (\boldsymbol{\omega}_{B/I} \times \boldsymbol{r}_{P\to D}) + \boldsymbol{F}_A/m_P][m_D m_P/(m_D + m_P)] \tag{22}$$

The rotational kinetic equations of motion for the projectile and disk bodies are given by

$$\frac{{}^I \mathrm{d}\boldsymbol{H}_{D/I}}{\mathrm{d}t} = \boldsymbol{M}_R \tag{23}$$

$$\frac{{}^I \mathrm{d}\boldsymbol{H}_{P/I}}{\mathrm{d}t} = -\boldsymbol{M}_R - \boldsymbol{r}_{P\to D} \times \boldsymbol{F}_R + \boldsymbol{M}_A \tag{24}$$

Summing the preceding two equations eliminates the reaction moment and forms the rotational kinetic equation for the two-body system expressed in the body reference frame,

$$\frac{{}^I \mathrm{d}\boldsymbol{H}_{P/I}}{\mathrm{d}t} + \frac{{}^I \mathrm{d}\boldsymbol{H}_{D/I}}{\mathrm{d}t} = -\boldsymbol{r}_{P\to D} \times \boldsymbol{F}_R + \boldsymbol{M}_A \tag{25}$$

Unlike the kinetic translational equation of motion, it is easier to form the rotational equation of motion in the body frame and later convert it to the no-roll reference frame when it is expressed in component form. Therefore, the angular momentum derivatives are expressed as

$$\frac{{}^I \mathrm{d}\boldsymbol{H}_{D/I}}{\mathrm{d}t} = \frac{{}^B \mathrm{d}\boldsymbol{H}_{D/I}}{\mathrm{d}t} + \omega_{B/I} \times \boldsymbol{H}_{D/I} \tag{26}$$

$$\frac{{}^I \mathrm{d}\boldsymbol{H}_{P/I}}{\mathrm{d}t} = \frac{{}^B \mathrm{d}\boldsymbol{H}_{P/I}}{\mathrm{d}t} + \omega_{B/I} \times \boldsymbol{H}_{P/I} \tag{27}$$

The translational dynamic equation given in Eq. (15) is expressed in the no-roll frame,

$$\begin{Bmatrix} \dot{\tilde{u}} \\ \dot{\tilde{v}} \\ \dot{\tilde{w}} \end{Bmatrix} = \frac{1}{m_C} \begin{Bmatrix} \tilde{X} \\ \tilde{Y} \\ \tilde{Z} \end{Bmatrix} - \begin{bmatrix} 0 & -\tilde{r} & \tilde{q} \\ \tilde{r} & 0 & \tilde{r} t_\theta \\ -\tilde{q} & -\tilde{r} t_\theta & 0 \end{bmatrix} \begin{Bmatrix} \tilde{u} \\ \tilde{v} \\ \tilde{w} \end{Bmatrix} \tag{28}$$

where the weight force and aerodynamic loads expressed in the no-roll frame are

$$\boldsymbol{F}_A = \tilde{X}_A \boldsymbol{I}_N + \tilde{Y}_A \boldsymbol{J}_N + \tilde{Z}_A \boldsymbol{K}_N \tag{29}$$

$$\boldsymbol{W}_C = \tilde{X}_W \boldsymbol{I}_N + \tilde{Y}_W \boldsymbol{J}_N + \tilde{Z}_W \boldsymbol{K}_N \tag{30}$$

so that

$$\begin{Bmatrix} \tilde{X} \\ \tilde{Y} \\ \tilde{Z} \end{Bmatrix} = \begin{Bmatrix} \tilde{X}_A \\ \tilde{Y}_A \\ \tilde{Z}_A \end{Bmatrix} + \begin{Bmatrix} \tilde{X}_W \\ \tilde{Y}_W \\ \tilde{Z}_W \end{Bmatrix} \tag{31}$$

where

$$\begin{Bmatrix} \tilde{X}_W \\ \tilde{Y}_W \\ \tilde{Z}_W \end{Bmatrix} = m_C g \begin{Bmatrix} -s_\theta \\ 0 \\ c_\theta \end{Bmatrix} \tag{32}$$

The aerodynamic forces are described in the next section.

The body frame components of the rotational dynamics equation of motion given by Eq. (25) can be written as

$$[A_{\mathrm{RD}}] \begin{Bmatrix} \dot{p} \\ \dot{q} \\ \dot{r} \end{Bmatrix} = \{B_{\mathrm{RD}}\} \tag{33}$$

where

$$A_{\mathrm{RD}} = I_P + T_D I_D T_D^T - m_S S_{\mathrm{RPD}} S_{\mathrm{RPD}} \tag{34}$$

$$B_{\mathrm{RD}} = \begin{Bmatrix} L_A \\ M_A \\ N_A \end{Bmatrix} - m_S S_{\mathrm{RPD}} S_\omega S_\omega \begin{Bmatrix} x_{\mathrm{PD}} \\ y_{\mathrm{PD}} \\ z_{\mathrm{PD}} \end{Bmatrix} - \frac{m_S}{m_P} S_{\mathrm{RPD}} \begin{Bmatrix} X_A \\ Y_A \\ Z_A \end{Bmatrix} - S_\omega I_P \begin{Bmatrix} p \\ q \\ r \end{Bmatrix} - T_D I_D T_D^T S_\omega \begin{Bmatrix} n_x\Omega \\ n_y\Omega \\ n_z\Omega \end{Bmatrix} - S_\omega T_D I_D T_D^T \begin{Bmatrix} p + n_x\Omega \\ q + n_y\Omega \\ r + n_z\Omega \end{Bmatrix} \tag{35}$$

$$S_{\mathrm{RPD}} = \begin{bmatrix} 0 & -z_{\mathrm{PD}} & y_{\mathrm{PD}} \\ z_{\mathrm{PD}} & 0 & -x_{\mathrm{PD}} \\ -y_{\mathrm{PD}} & x_{\mathrm{PD}} & 0 \end{bmatrix} \tag{36}$$

$$[S_\omega] = \begin{bmatrix} 0 & -r & q \\ r & 0 & -p \\ -q & p & 0 \end{bmatrix} \tag{37}$$

The transformation matrix from the disk reference frame to the projectile reference frame is formed as

$$\begin{Bmatrix} \boldsymbol{I}_B \\ \boldsymbol{J}_B \\ \boldsymbol{K}_B \end{Bmatrix} = \begin{bmatrix} c_{\theta_D} & 0 & s_{\theta_D} \\ s_{\phi_D} s_{\theta_D} & c_{\phi_D} & -s_{\phi_D} c_{\theta_D} \\ -c_{\phi_D} s_{\theta_D} & s_{\phi_D} & c_{\phi_D} c_{\theta_D} \end{bmatrix} \begin{Bmatrix} \boldsymbol{I}_D \\ \boldsymbol{J}_D \\ \boldsymbol{K}_D \end{Bmatrix} = [T_D] \begin{Bmatrix} \boldsymbol{I}_D \\ \boldsymbol{J}_D \\ \boldsymbol{K}_D \end{Bmatrix} \tag{38}$$

To be consistent with projectile linear theory, Eq. (33) is converted to the no-roll frame through multiplication of the equation by T_ϕ^T. Also, a change of variables is introduced from body frame angular velocity components to no-roll frame components. With these conversions, Eq. (33) is expressed as

$$[\tilde{A}_{\mathrm{RD}}] \begin{Bmatrix} \dot{\tilde{p}} \\ \dot{\tilde{q}} \\ \dot{\tilde{r}} \end{Bmatrix} = \{\tilde{B}_{\mathrm{RD}}\} \tag{39}$$

where

$$\tilde{A}_{\mathrm{RD}} = T_\phi^T \left(I_P + T_D I_D T_D^T - m_S S_{\mathrm{RPD}} S_{\mathrm{RPD}} \right) T_\phi \tag{40}$$

$$\tilde{B}_{\mathrm{RD}} = \begin{Bmatrix} \tilde{L}_A \\ \tilde{M}_A \\ \tilde{N}_A \end{Bmatrix} - m_S T_\phi^T S_{\mathrm{RPD}} S_\omega S_\omega \begin{Bmatrix} x_{\mathrm{PD}} \\ y_{\mathrm{PD}} \\ z_{\mathrm{PD}} \end{Bmatrix} - \frac{m_S}{m_P} T_\phi^T S_{\mathrm{RPD}} \begin{Bmatrix} \tilde{X}_A \\ \tilde{Y}_A \\ \tilde{Z}_A \end{Bmatrix} - T_\phi^T S_\omega I_P T_\phi \begin{Bmatrix} \tilde{p} \\ \tilde{q} \\ \tilde{r} \end{Bmatrix} - T_\phi^T T_D I_D T_D^T S_\omega \begin{Bmatrix} n_x\Omega \\ n_y\Omega \\ n_z\Omega \end{Bmatrix} - T_\phi^T S_\omega T_D I_D T_D^T T_\phi \begin{Bmatrix} \tilde{p} \\ \tilde{q} \\ \tilde{r} \end{Bmatrix} - T_\phi^T S_\omega T_D I_D T_D^T \begin{Bmatrix} n_x\Omega \\ n_y\Omega \\ n_z\Omega \end{Bmatrix} - T_\phi^T \left(I_P + T_D I_D T_D^T - m_S S_{\mathrm{RPD}} S_{\mathrm{RPD}} \right) \dot{T}_\phi \begin{Bmatrix} \tilde{p} \\ \tilde{q} \\ \tilde{r} \end{Bmatrix} \tag{41}$$

$$T_\phi = \begin{bmatrix} 1 & 0 & 0 \\ 0 & c_\phi & s_\phi \\ 0 & -s_\phi & c_\phi \end{bmatrix} \tag{42}$$

$$\dot{T}_\phi = (\tilde{p} + t_\theta \tilde{r}) \begin{bmatrix} 0 & 0 & 0 \\ 0 & -s_\phi & c_\phi \\ 0 & -c_\phi & -s_\phi \end{bmatrix} \tag{43}$$

In the preceding cross product operator matrix S_ω, the body frame angular velocity components p, q, and r are replaced by $\tilde{p}$, $c_\phi \tilde{q} + s_\phi \tilde{r}$, and $-s_\phi \tilde{q} + c_\phi \tilde{r}$, respectively.

Equations (11), (12), (28), and (39) provide 12 nonlinear differential equations that govern atmospheric flight of a projectile equipped with an axisymmetric rotating internal component. With a given set of initial conditions, these equations can be numerically integrated forward in time.

Aerodynamic Forces and Moments

The equations of motion discussed earlier are largely driven by the aerodynamic forces and moments exerted on the projectile body. The aerodynamic loads consist of steady aerodynamic forces and linear Magnus forces and are formulated separately,

$$\begin{Bmatrix} \tilde{X}_A \\ \tilde{Y}_A \\ \tilde{Z}_A \end{Bmatrix} = \begin{Bmatrix} \tilde{X}_S \\ \tilde{Y}_S \\ \tilde{Z}_S \end{Bmatrix} + \begin{Bmatrix} \tilde{X}_M \\ \tilde{Y}_M \\ \tilde{Z}_M \end{Bmatrix} \tag{44}$$

The steady aerodynamic forces act at the center of pressure of the projectile body and are

$$\begin{Bmatrix} \tilde{X}_S \\ \tilde{Y}_S \\ \tilde{Z}_S \end{Bmatrix} = -q_\alpha \begin{Bmatrix} C_{X0} + C_{X2}\alpha^2 + C_{X2}\beta^2 \\ C_{Y0} + C_{YB1}\beta \\ C_{Z0} + C_{ZB1}\alpha \end{Bmatrix} \tag{45}$$

The Magnus force act at the Magnus force center of pressure, which is different from the center of pressure of the steady aerodynamic forces. Figure 3 shows the relative locations of the projectile body centers of pressure.

$$\begin{Bmatrix} \tilde{X}_M \\ \tilde{Y}_M \\ \tilde{Z}_M \end{Bmatrix} = q_\alpha \begin{Bmatrix} 0 \\ \dfrac{\tilde{p} D C_{YPA} \alpha}{2V} \\ -\dfrac{\tilde{p} D C_{YPA} \beta}{2V} \end{Bmatrix} \tag{46}$$

The longitudinal and lateral aerodynamic angles of attack used in Eqs. (45) and (46) are

$$\alpha = \tan^{-1}(\tilde{w}/\tilde{u}) \cong \tilde{w}/\tilde{u}, \qquad \beta = \tan^{-1}(\tilde{v}/\tilde{u}) \cong \tilde{v}/\tilde{u} \tag{47}$$

$$q_\alpha = (\pi/8)\rho D^2(\tilde{u}^2 + \tilde{v}^2 + \tilde{w}^2) \tag{48}$$

Aerodynamic coefficients in Eqs. (45) and (46) depend on local Mach number at the composite body mass center.

The externally applied moments on the projectile body found on the right-hand side of the rotational kinetic equations contain contributions from steady and unsteady aerodynamics and Magnus moments,

$$\begin{Bmatrix} \tilde{L}_A \\ \tilde{M}_A \\ \tilde{N}_A \end{Bmatrix} = \begin{Bmatrix} \tilde{L}_S \\ \tilde{M}_S \\ \tilde{N}_S \end{Bmatrix} + \begin{Bmatrix} \tilde{L}_U \\ \tilde{M}_U \\ \tilde{N}_U \end{Bmatrix} + \begin{Bmatrix} \tilde{L}_M \\ \tilde{M}_M \\ \tilde{N}_M \end{Bmatrix} \tag{49}$$

The steady aerodynamic moments are computed for the projectile body with a cross product between the steady body aerodynamic force vector and the distance vector from the projectile center of gravity to the center of pressure. Magnus moments on the body are computed in a similar way, with a cross product between the Magnus force vector and the distance vector from the projectile center of gravity to the Magnus center of pressure. The unsteady

body aerodynamic moments provide a damping source for projectile angular motion and are given by

$$\begin{Bmatrix} \tilde{L}_U \\ \tilde{M}_U \\ \tilde{N}_U \end{Bmatrix} = \tilde{\gamma}_\alpha D \begin{Bmatrix} C_{DD} + \dfrac{\tilde{p} D C_{LP}}{2V} \\ \dfrac{\tilde{q} D C_{MQ}}{2V} \\ \dfrac{\tilde{r} D C_{NR}}{2V} \end{Bmatrix} \tag{50}$$

Air density is computed using the standard atmosphere.[13]

Rotating Internal Part Projectile Linear Theory

The preceding equations of motion in their current state are highly nonlinear and whereas a solution, given an initial set of conditions, may be obtained numerically, it is desirable to solve them with a closed-form solution for increased understanding of the dynamic behavior. Linear theory for symmetric rigid projectiles introduces a series of assumptions that yield a refined set of linear differential equations that can be solved in closed form. These equations form the basis of classic projectile stability theory. This same set of assumptions can be used to establish a linear theory for projectiles containing an axisymmetric rotating internal part in atmospheric flight. The necessary assumptions are as follows.

1) The variable is changed from no-roll, station line velocity u, to total velocity V. V and u and their derivatives are related as

$$V = \sqrt{\tilde{u}^2 + \tilde{v}^2 + \tilde{w}^2} \tag{51}$$

$$\dot{V} = (\tilde{u}\dot{\tilde{u}} + \tilde{v}\dot{\tilde{v}} + \tilde{w}\dot{\tilde{w}})/V \tag{52}$$

2) The variables are changed from time t to dimensionless arc length s. The dimensionless arc length, as defined by Murphy,[14] is given next and is measured in units of distance traveled,

$$s = \frac{1}{D}\int_0^t V \, \mathrm{d}\tau \tag{53}$$

Time and arc length derivatives of a dummy variable ζ are related by

$$\dot{\zeta} = (V/D)\zeta' \tag{54}$$

$$\ddot{\zeta} = (V/D)^2(\zeta'' + \zeta' V'/V) \tag{55}$$

3) Euler yaw and pitch angles are small,

$$s_\theta \approx \theta, \qquad c_\theta \approx 1, \qquad s_\psi \approx \psi, \qquad c_\psi \approx 1 \tag{56}$$

4) Aerodynamic angles of attack are small,

$$\alpha \approx \tilde{w}/V \qquad \beta \approx \tilde{v}/V \tag{57}$$

5) The effects of mass and inertia changes of a projectile on stability are well known. To evaluate properly the affects on stability solely due to a rotating internal part, the total mass of the two-component system is held constant and individual component mass and inertia properties are appropriately modified. Beginning with a symmetric projectile, a disk is removed from the rigid projectile body and replaced with a rotating disk that has the same mass and inertia properties as the removed portion. Hence, the two-body system has its mass center along the axis of symmetry. For computing aerodynamic loads, the velocity of the original rigid-body mass center, along the axis of symmetry of the projectile, is used and not the projectile body mass center, which for offset disk configurations, oscillates at the projectile spin rate. The shift in the projectile's center of gravity due to the addition of the internal part is

$$\begin{Bmatrix} x_P \\ y_P \\ z_P \end{Bmatrix} = \frac{1}{m_P} \begin{Bmatrix} m_E x_E - m_D x_D \\ m_E y_E - m_D y_D \\ m_E z_E - m_D z_D \end{Bmatrix} \tag{58}$$

The projectile's inertia matrix for various disk configurations is populated by

$$I_P = I_E - m_P \begin{bmatrix} y_P^2 + z_P^2 & x_P y_P & x_P z_P \\ x_P y_P & x_P^2 + z_P^2 & y_P z_P \\ x_P z_P & y_P z_P & x_P^2 + y_P^2 \end{bmatrix}$$
$$- T_D I_D T_D^T - m_D \begin{bmatrix} y_D^2 + z_D^2 & x_D y_D & x_D z_D \\ x_D y_D & x_D^2 + z_D^2 & y_D z_D \\ x_D z_D & y_D z_D & x_D^2 + y_D^2 \end{bmatrix} \tag{59}$$

where

$$m_P = m_E - m_D \tag{60}$$

6) The projectile is aerodynamically symmetric.

$$C_{NR} = C_{MQ} \tag{61}$$

$$C_{Y0} = C_{Z0} = 0 \tag{62}$$

$$C_{YB1} = C_{ZB1} = C_{NA} \tag{63}$$

7) A flat fire trajectory is assumed, and the force of gravity is neglected for stability analysis.

8) The quantities θ, ψ, $\tilde{q}$, $\tilde{r}$, $\tilde{v}$, and $\tilde{w}$ are small compared to V and ϕ; therefore, the products of these small quantities and their derivatives are negligible.

After application of these assumptions, the projectile linear theory differential equations are obtained,

$$x' = D \tag{64}$$

$$y' = \left(\frac{D}{V}\right)\tilde{v} + \psi D \tag{65}$$

$$z' = \left(\frac{D}{V}\right)\tilde{w} - \theta D \tag{66}$$

$$\phi' = \left(\frac{D}{V}\right)\tilde{p} \tag{67}$$

$$\theta' = \left(\frac{D}{V}\right)\tilde{q} \tag{68}$$

$$\psi' = \left(\frac{D}{V}\right)\tilde{r} \tag{69}$$

$$V' = -\frac{(\rho S D C_{X0} V)}{2m_C} \tag{70}$$

$$p' = \left[\frac{\rho S D^2 (D C_{LP}\tilde{p} + 2C_{DD}V)}{4(I_{DXX} + I_{PXX})}\right] \tag{71}$$

$$\begin{Bmatrix} v' \\ w' \\ q' \\ r' \end{Bmatrix} = \begin{bmatrix} A & 0 & 0 & -D \\ 0 & A & D & 0 \\ B & C & E & -F \\ -C & B & F & E \end{bmatrix} \begin{Bmatrix} \tilde{v} \\ \tilde{w} \\ \tilde{q} \\ \tilde{r} \end{Bmatrix} + \boldsymbol{F}_F \tag{72}$$

Equations (64–72) are linear, except for the total velocity V, which is retained in several of the equations. It is assumed that V changes slowly with respect to the other state variables and is considered to be constant where it appears in other dynamic equations. With this assumption, the total velocity, the angle-of-attack dynamics, and the roll dynamics all become uncoupled, linear-time-invariant equations of motion.

Equation (72) is the matrix form of the epicyclic dynamic equations where $\boldsymbol{F}_F$ is a periodic inhomogeneous forcing term. The angle-of-attack stability of the projectile is largely determined by the homogeneous equations. Note that the basic structure of the

epicyclic dynamic equations of a rigid projectile are the same as shown earlier. Differences in the epicyclic dynamics of both configurations are contained in the coefficients B, C, E, and F. In the most general case, where the disk is located off the axis of symmetry and canted at an arbitrary angle, these coefficients are algebraically lengthy. Although straightforward and computationally trivial to compute, space limitations here prevent the most general form of these coefficients to be listed. However, the Appendix provides these coefficients for the special case of the disk located on and aligned with the projectile axis of symmetry.

The four roots of the homogeneous characteristic equation shown in Eq. (72) are given as

$$s = \begin{Bmatrix} \frac{1}{2}\Big[A+E-iF \\ \qquad \pm\sqrt{(A-E)^2+4CD-F^2+2i(AF-2BD-EF)}\Big] \\ \frac{1}{2}\Big[A+E+iF \\ \qquad \pm\sqrt{(A-E)^2+4CD-F^2+2i(EF+2BD-AF)}\Big] \end{Bmatrix} \tag{73}$$

Two complex roots are generated, which are typically called the epicyclic fast and slow modes. These results are identical to conventional rigid projectile analysis. Consequently, rotating internal part projectile analysis can be approached in essentially the same manner that rigid projectiles are analyzed.

Example Results

To examine the changes an internal rotating disk induces on the dynamic behavior of a projectile, the following analysis documents how the fast and slow epicyclic modes change for various rotating disk arrangements. Results are shown for a typical 155-mm spin-stabilized artillery shell having a nominal weight of 94.88 lbf with a reference area of $S = 0.20$ ft^2 and a reference diameter $D = 0.51$ ft. The nominal stationline, buttline, and waterline distances to the projectile's center of gravity are $x_E = 1.06$ ft, $y_E = 0.00$ ft, and $z_E = 0.00$ ft. The air density is specified at $\rho = 1.75E{-}3$ slugs $\cdot$ ft^3, and aerodynamic coefficients are $C_{NA} = 2.66$, $C_{YPA} = -0.96$, and $C_{MQ} = -27.7$. The standard aerodynamic center of pressure and the aerodynamic center of Magnus are located at the following distances along the stationline, buttline, and waterline $x_A = 1.76$ ft, $y_A = 0.00$ ft, and $z_A = 0.00$ ft and $x_M = 1.76$ ft, $y_M = 0.00$ ft, and $z_M = 0.00$ ft. The moments of inertia about the body axis are $I_{EXX} = 0.11$, $I_{EYY} = 1.40$, and $I_{EZZ} = 1.40$ slug $\cdot$ ft^2. The nominal disk is 0.33 ft in diameter, 0.06 ft thick, and weighs 9.5 lbf. It is nominally located on the projectile center of gravity and has the following inertia properties: $I_{DXX} = 0.0041$, $I_{DYY} = 0.0021$, and $I_{DZZ} = 0.0021$ slug $\cdot$ ft^2. Euler angles of the projectile are $\varphi = 0.00$ rad, $\theta = 0.00$ rad, and $\psi = 0.00$ rad. The projectile has a forward velocity of $\tilde{u} = 2710$ ft/s and a spin rate of $\tilde{p} = 1674.10$ rad/s. The pitch and yaw rates and the side velocities are all equal to zero. The disk spin rate and orientation relative to the projectile are varied.

In the analysis to follow, the ratio of the disk mass to projectile mass is dubbed the mass ratio M_R, the ratio of the disk spin rate to the projectile spin rate is call the spin ratio S_R, the angle that the disk is rotated from the projectile axis is given as the disk angle φ_D, and the angle that the disk spin axis is nutated from the projectile axis is given as the disk angle θ_D. The disk rotation and nutation angles are defined in Fig. 1.

A mass ratio of 1/20 and a spin ratio of 10 were considered for a system containing a disk located on the projectile center of gravity. The orientation of the disk is located by a rotation of ϕ_D about $\boldsymbol{I}_B$, followed by a rotation of θ_D about $\boldsymbol{J}_D$. Because the projectile is symmetrical, the rotation angle ϕ_D of the disk has no physical significance on the configuration of the system and cannot affect the stability. Thus, the epicyclic modes are solely a function of the nutation angle θ_D, which is the angle between the spin axes of the disk and spin axes of the projectile. The angle between the spin axes of the disk and the spin axes of the projectile was varied over a range from 0 to 360 deg, and the natural frequencies and damping ratio factors for this system were determined and are shown for the fast and slow modes in Figs. 4 and 5. Figures 4 and 5 show that the eigenvalues of the system's epicyclic equations are dependent on disk orientation. It is also shown that orientation angles that affect a relatively large change in natural frequency have very little effect on the damping of the system. The converse is true as well. Moreover, Fig. 5 shows that if it is desired for this particular system to remain stable certain disk orientation angles must be avoided.

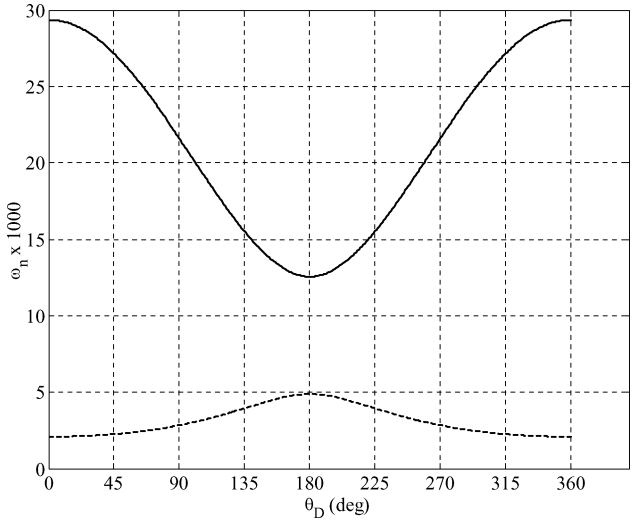

Fig. 4 System natural frequencies, mass ratio = 1/20, and spin ratio = 10.

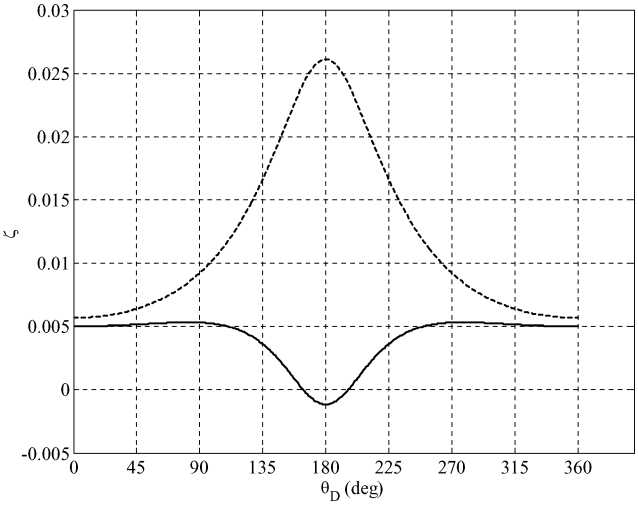

Fig. 5 Damping factors, mass ratio = 1/20, and spin ratio = 10.

The preceding study was repeated for a wide range of lateral disk displacements, and the exact set of eigenvalues was obtained for all positions. Thus, for a given disk-orientation the epicyclic dynamics of the system are independent of the lateral placement of the disk. In other words, no matter where the disk is placed with respect to the projectile, for a given disk orientation and the same set of flight conditions, the roots of the epicyclic equations will be exactly the same.

The root locus for various mass ratios and spin ratios is shown in Figs. 6–11. The disk nutation angle θ_D is varied from 0 (diamond) to 360 deg. The disk angle is defined in the inset of Fig. 6 for a disk located off the projectile axis of symmetry in the buttline direction ($\boldsymbol{J}_B$ axis). Because the epicyclic dynamics are independent of disk location, this lateral displacement was arbitrarily chosen

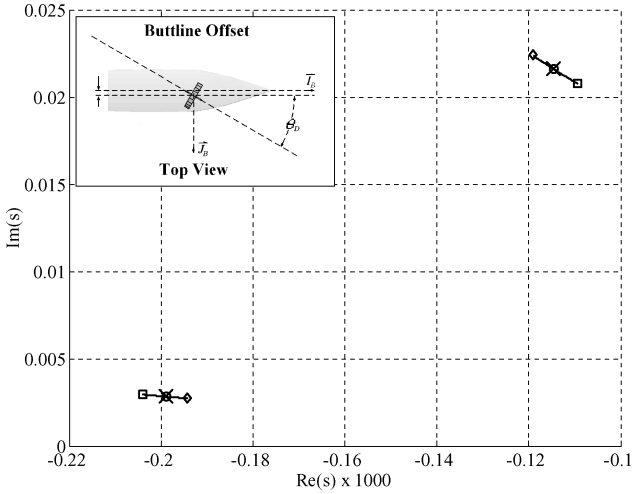

Fig. 6 Root locus for mass ratio = 1/100 and spin ratio = 5: ◇, $\theta_D = 0$, 360 deg; ○, $\theta_D = 90$ deg; □, $\theta_D = 180$ deg; and ×, rigid projectile.

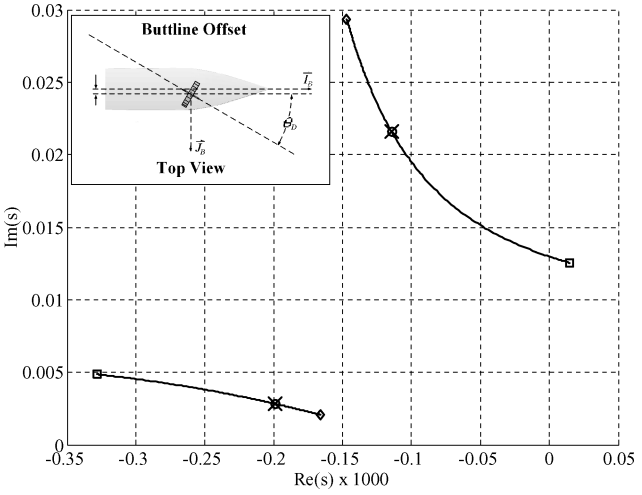

Fig. 7 Root locus for mass ratio = 1/10 and spin ratio = 5: ◇, $\theta_D = 0$, 360 deg; ○, $\theta_D = 90$ deg; □, $\theta_D = 180$ deg; and ×, rigid projectile.

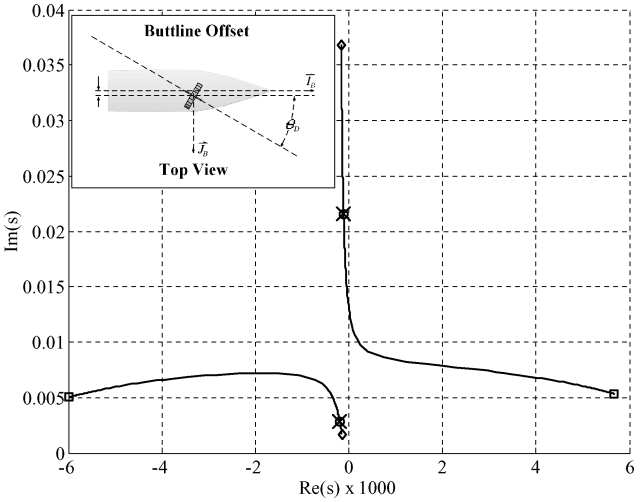

Fig. 8 Root locus for mass ratio = 1/5 and spin ratio = 5: ◇, $\theta_D = 0$, 360 deg; ○, $\theta_D = 90$ deg; □, $\theta_D = 180$ deg; and ×, rigid projectile.

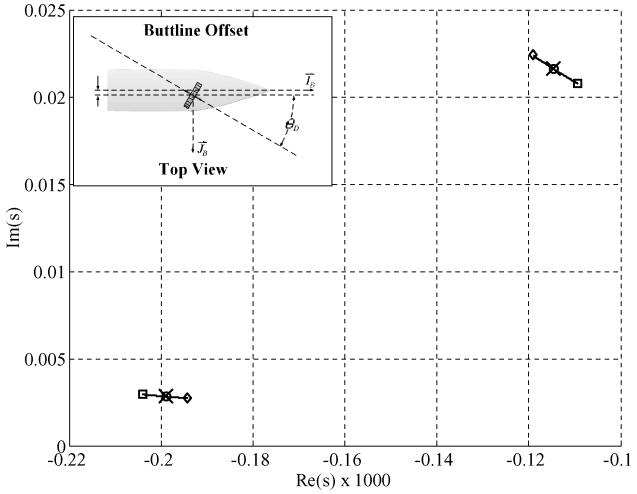

Fig. 9 Root locus for spin ratio = 1/2 and mass ratio = 1/10: ◇, $\theta_D = 0$, 360 deg; ○, $\theta_D = 90$ deg; □, $\theta_D = 180$ deg; and ×, rigid projectile.

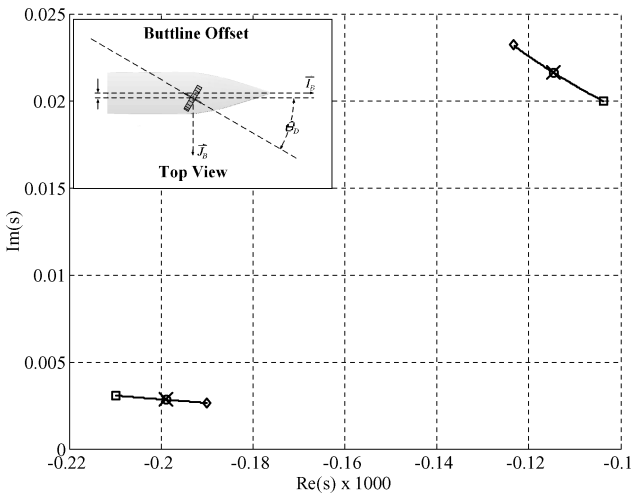

Fig. 10 Root locus for spin ratio = 1 and mass ratio = 1/10: ◇, $\theta_D = 0$, 360 deg; ○, $\theta_D = 90$ deg; □, $\theta_D = 180$ deg; and ×, rigid projectile.

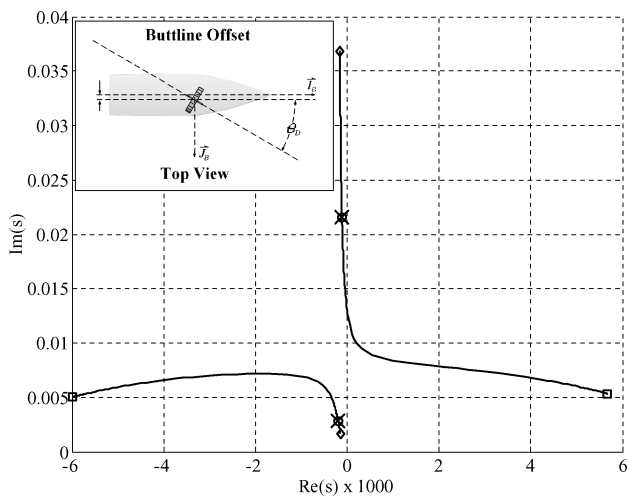

Fig. 11 Root locus for spin ratio = 10 and mass ratio = 1/10: ◇, $\theta_D = 0$, 360 deg; ○, $\theta_D = 90$ deg; □, $\theta_D = 180$ deg; and ×, rigid projectile.

as a representative case to study the effects that varying the mass and spin ratios have on the epicyclic dynamics. The circle indicates the eigenvalues for a disk angle of 90 deg, the square for a disk angle of 180 deg, and the bold × the location of the eigenvalues determined from a similar rigid artillery round without a rotating internal part. These conventions are used throughout. In Figs. 6–11, the epicyclic modes travel from the diamond to the square as the disk angle is increased from 0 to 180 deg and march back up the same path toward the diamond as the disk angle is further increased from 180 to 360 deg. In Fig. 6, it can be seen that a disk of mass ratio 1/100 slightly affects the projectile fast and slow modes at angles other than 90 deg. The effect on the epicyclic dynamics of the system of varying the disk orientation for three different mass ratios with a spin ratio of 5 is demonstrated in the root-locus plots shown in Figs. 8–10. Comparison of Figs. 8–10 reveals that increasing the mass ratio increases the effect that the spinning disk has on the epicyclic dynamics. As shown in Fig. 8, when the mass ratio is sufficiently large, the fast mode can become unstable for large disk angles greater than 90 deg. In this case, spin stability of the complete round is adversely impacted by the $\boldsymbol{I}_B$ component of disk angular velocity in the opposite direction of projectile spin. Also note that the mass ratio has very little effect on the stability of the system for a disk angle of 90 deg. For disk angles greater than 180 deg, the eigenvalues march back along the same path toward 0 deg. This is expected because for a disk located on the projectile axis of symmetry the disk angles from 0 to 180 deg relative to the projectile are equivalent to the angles from 180 to 360 deg with the direction of spin reversed.

Figures 9–11 are root-locus plots obtained by varying the disk angle for three different spin ratios with a disk to projectile mass ratio of 1/10. When Figs. 9–11 are compared, it is shown that decreasing spin ratio diminishes the effect that a spinning disk of a given mass has on the epicyclic modes. Increasing the spin ratio increases the dynamic effects and is capable of driving the system unstable for certain disk angles. Comparison of Figs. 6 and 9 and comparison of Figs. 8 and 11 show that the same dynamic effects can be achieved with either mass ratio or spin ratio. Note that if the product $M_R S_R$ is held constant the fast and slow modes do not change with disk location nor do they change for the same set of disk orientations. Figs. 6–11 also demonstrate that a disk of any mass ratio, spinning in the same direction as the projectile, that is, disk angle < 90 deg, tends to stabilize the fast mode of the system while destabilizing the slow mode. Disk angles of greater than 90 up to 180 deg have the opposite effect. However, for large spin ratios and large mass ratios, the movement of the modes is much greater per increase in disk angle. Note that the same plots, as those in Figs. 6–11, would be generated for the same conditions no matter where the disk was placed with respect to projectile body.

Conclusions

The equations of motion for a projectile containing an axisymmetric rotating internal disk that spins at a constant rate have been developed. The model allows for the disk to be located off the axis of symmetry of the projectile and oriented at arbitrary angles relative to the projectile axis of symmetry. Projectile linear theory has been modified to accommodate projectile configurations that contain an internal rotating disk. The addition of an internal rotating disk alters several of the coefficients in the epicyclic dynamic equations leading to modified fast and slow epicyclic modes.

With the use of modified projectile linear theory, the effect of disk orientation, location, mass, and speed is systematically studied. For a specified mass and spin ratio, the orientation of the disk affects the dynamics of the system; however, the location of the disk has no effect on the dynamics of the system. If the mass ratio times the spin ratio is held constant, then the same epicyclic modes are produced for a given set of disk orientations.

Appendix: Special Case Epicyclic Coefficients

Application of the linear theory assumptions to the simplified system of a projectile containing a rotating internal part located on the projectile axis of symmetry at a disk angle ψ_D equal to 0 deg yields the coefficients of the epicyclic equations as

$$A = -\frac{\rho S D C_{NA}}{2m_C} \tag{A1}$$

$$B = \left(\frac{\rho S D}{2m_C}\right)\left(\frac{m_C D}{I_{CYY}}\right)\left\{\frac{[x_{PM} - x_{\mathrm{PD}}(m_D/m_C)]C_{YPA}\tilde{p}}{2V}\right\} \tag{A2}$$

$$C = \left(\frac{\rho S D}{2m_C}\right)\left(\frac{m_C D}{I_{CYY}}\right)\left\{\frac{[x_{PA} - x_{\mathrm{PD}}(m_D/m_C)]C_{NA}}{2D}\right\} \tag{A3}$$

$$D = D \tag{A4}$$

$$E = \left(\frac{\rho S D}{2m_C}\right)\left(\frac{m_C D^2}{I_{CYY}}\right)\frac{C_{MQ}}{2} \tag{A5}$$

$$F = \left(\frac{D}{V}\right)\frac{I_{PXX}\tilde{p} + I_{DXX}(\tilde{p} + \Omega)}{I_{CYY}} \tag{A6}$$

Magnus force is assumed to be small in comparison to other aerodynamic forces and is dropped from Eqs. (A1–A6). However, because of the magnitude amplification resulting form the cross product between Magnus force and its respective moment arm, the Magnus moment is retained in Eq. (A2). The periodic forcing function $\boldsymbol{F}_F$ reduces to zero for the simplified case. The equations for the simplified system presented are essentially the same as those derived for a dual-spin projectile by Costello and Peterson.[11] They are identical if the aerodynamic coefficients applied on the aft section of a dual-spin projectile are neglected.

References

[1]Murphy, C., "Symmetric Missile Dynamic Instabilities," *Journal of Guidance, Control, and Dynamics*, Vol. 4, No. 5, 1981, pp. 464–471.

[2]Soper, W., "Projectile Instability Produced by Internal Friction," *AIAA Journal*, Vol. 16, No. 1, 1978, pp. 8–11.

[3]Murphy, C., "Influence of Moving Internal Parts on Angular Motion of Spinning Projectiles," *Journal of Guidance, Control, and Dynamics*, Vol. 1, No. 2, 1978, pp. 117–122.

[4]D'Amico, W., "Comparison of Theory and Experiment for Moments Induced by Loose Internal Parts," *Journal of Guidance, Control, and Dynamics*, Vol. 10, No. 1, 1987, pp. 14–19.

[5]Hodapp, A., "Passive Means for Stabilizing Projectiles with Partially Restrained Internal Members," *Journal of Guidance, Control, and Dynamics*, Vol. 12, No. 2, 1989, pp. 135–139.

[6]Goddard, R., "Apparatus for Steering Aircraft," U.S. Patent 2594766, April 1952.

[7]Barrett, R., and Stutts, J., "Modeling, Design, and Testing of a Barrel-Launched Adaptive Munition," *Proceedings of the 4th Annual Society of Photo-Optical Engineers Symposium on Smart Structures*, Society of Photo-Optical Engineers, New York, 1997.

[8]Schmidt, E., and Donovan, W., "Technique to Reduce Yaw and Jump of Fin-Stabilized Projectiles," *Journal of Spacecraft and Rockets*, Vol. 35, No. 1, 1998, pp. 110, 111.

[9]Costello, M., and Agarwalla, R., "Improved Dispersion of a Fin Stabilized Projectile Using a Passive Moveable Nose," *Journal of Guidance, Control, and Dynamics*, Vol. 23, No. 5, 2000, pp. 900–903; Errata, Vol. 25, No. 2, 2002, p. 414.

[10]Smith, J., Smith, K., and Topliffe, R., "Feasibility Study for Application of Modular Guidance and Control Units to Existing ICM Projectiles," Final Technical Report, Contractor Rept. ARLCD-CR-79001, U.S. Army Armament Research and Development Command, Picatinny Arsenal, Dover, NJ, 1978.

[11]Costello, M., and Peterson, A., "Linear Theory of a Dual Spin Projectile in Atmospheric Flight," *Journal of Guidance, Control, and Dynamics*, Vol. 23, No. 4, 2000, pp. 789–797.

[12]Burchett, B., Peterson, A., and Costello, M., "Prediction of Swerving Motion of a Dual-Spin Projectile with Lateral Pulse Jets in Atmospheric Flight," *Mathematical and Computer Modeling*, Vol. 35, No. 7–8, 2002, pp. 821–834.

[13]Von Mises, R., *Theory of Flight*, Dover, New York, 1959, Chap. 1.

[14]Murphy, C. H., "Free Flight Motion of Symmetric Missiles," U.S. Army Research Lab., Rept. 1216, Aberdeen Proving Ground, MD, July 1963.